Influence of the Laser Incidence Conditions on the Spontaneous Polarization Reorientation Photorefractive Effect of Ferroelectric Liquid Crystals

Takeo Sasaki,* Oki Mochizuki, Kazunori Noborio, and Yukihito Nakazawa

Department of Chemistry, Faculty of Science, Science University of Tokyo, 1-3 Kagurazaka, Shinjuku-ku, Tokyo 162-8601, Japan

Received: June 7, 2004

The photorefractivity of a ferroelectric liquid crystal (FLC) mixed with a photoconductive compound was investigated in detail. FLCs are anisotropic media, so that laser beam incidence conditions strongly affect the formation of the refractive index grating. Effects of intersection angles of the laser beams, sample angle, sample rotation angle, sample thickness, and polarization of the laser beams on the photorefractivity of FLCs were examined.

Introduction

The photorefractive effect is a phenomenon in which the change in refractive index is induced by a combined mechanism of photovoltaic and electrooptic effects.[1−4] Materials that exhibit both photoconductivity and electrooptic effects have potential use as photorefractive materials. The photorefractive effect of organic materials, such as glassy polymers,[3−8] low-molecular-weight liquid crystals,[9−18] liquid crystalline polymers,[19,20] and amorphous compounds,[21,22] have been reported since 1990.

The change in refractive index through the photorefractive effect occurs only within the interference fringe of the incident laser beams. When laser beams interfere in a photorefractive material, charge separation occurs between the light and the dark positions of the interference fringe. A space-charge field (internal electric field) is built at the area between the light and the dark positions. The refractive index of the corresponding area is changed through electrooptic effects. Thus, a refractive index grating is formed at the interference fringe. Dynamic volume holograms are easily formed through the photorefractive effect and this effect has direct applicability in photonics, including optical image processing, parallel optical logic, pattern recognition, and phase conjugation.

Recently, the photorefractivity of surface-stabilized ferroelectric liquid crystals (SS-FLCs) doped with a photoconductive compound has been investigated.[14−18] The FLCs exhibit photorefractivity only at the temperature where the LCs exhibit a ferroelectric phase (Sc* phase). The internal electric field alters the direction of spontaneous polarization at the area between the light and the dark positions of the interference fringe, which causes a periodic change in the orientations of FLC molecules. This is different from the processes that occur in other photorefractive materials, in that the molecular dipole, rather than the bulk polarization, responds to the internal electric field. The response time (refractive index grating formation time) was measured as 20−30 ms.[15,16,18]

In previous work by the present authors, influence of the properties of FLCs on the photorefractivity have been investigated.[18] It was revealed that the magnitude of the gain coefficient, response time, and stability of the two-beam coupling signal are strongly affected by the properties of FLCs, especially by the homogeneity of the surface-stabilized state. Superior photorefractive properties are obtained in SS-FLCs with higher homogeneity, that is, with fewer defects. Since SS-FLC films exhibit very high optical anisotropy, the beam incidence conditions (incidence angle, polarization direction, etc.) strongly affect the photorefractivity. In this study, the influence of the beam incidence conditions on the photorefractive effect of FLCs was investigated. The influence of the film thickness of FLCs was also examined.

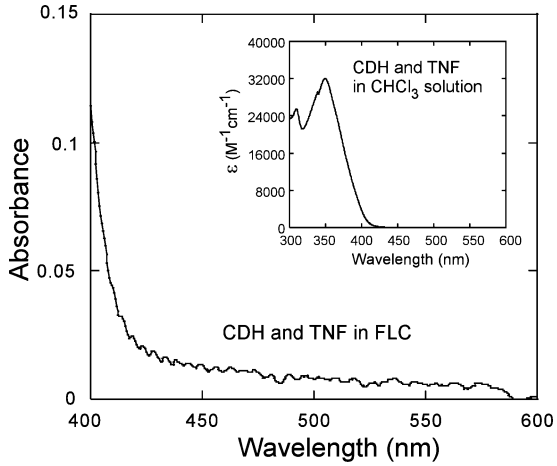

Figure 1. Absorption spectrum of CDH and TNF in an FLC (SCE8) medium measured in a 10-μm-gap LC cell. The concentration of CDH was 2 wt % and TNF was 0.1 wt %. The absorption of FLC was subtracted. Inset shows the absorption spectrum of a chloroform solution of CDH (2.5×10^{-5} mol/L) and TNF (1.3×10^{-6} mol/L).

Experimental Section

Samples. The FLC mixture used in this study was obtained commercially (FELIX SCE8, Clariant Japan Co.). The physical properties of SCE8 are listed in Table 1. A photoconductive compound, 9-ethyl-3-carbazolcarboxyaldehyde diphenylhydrazone (CDH), and a sensitizer, 2,4,7-trinitro-9-fluorenone (TNF), were mixed with the FLC. The concentration of CDH in the FLC was 2 wt % and that of TNF was 0.1 wt %. The absorption spectrum of the mixture is shown in Figure 1. CDH/TNF in

* To whom correspondence should be addressed. E-mail: sasaki@rs.kagu.tus.ac.jp.

10.1021/jp040415x CCC: $27.50
Published on Web 10/07/2004

TABLE 1: Physical Properties of the FLC Used in This Study

FLC	Ps at 25 °C nC/cm^2)	phase transition temperature[a] (°C)	response time[b] (μs)	rotational viscosity (mPas)	tilt angle (deg)
SCE8	−4.5	−Sc* 60 S_A 80 N* 104 I	50	76	20

[a] C, crystal; Sc*, chiral smectic C phase; S_A, smectic A phase; N*, chiral nematic phase; I, isotropic phase. [b] Response time to 10 V/μm electric field at 25 °C in a 2-μm cell.

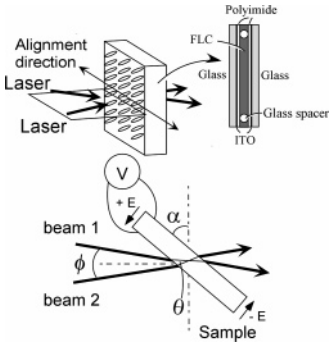

Figure 2. Schematic illustration of the beam incidence geometries.

the FLC medium showed absorption maximum at a wavelength around 350 nm. The absorbance at 450∼500 nm was sufficiently small to establish a Bragg diffraction grating.[3] The FLCs and dopants were dissolved in dichloroethane and the solvent was evaporated. The mixture was then dried in a vacuum at room temperature for one week. The samples were injected into a liquid crystal (LC) cell, as shown in Figure 2, equipped with 1 cm^2 indium-doped tin oxide (ITO) electrodes and a polyimide alignment layer (LX-1400, Hitachi Chemicals Co., parallel rubbing). The thickness of the FLC films was determined by the gap of the cell. Cells with gaps of 5, 10, 15, and 25 μm were used in this study.

The helical structure of the Sc* phase uncoils in the cell and forms a surface-stabilized state. To form a highly homogeneous surface-stabilized state, the samples are heated to the isotropic phase temperature and deliberately cooled to the SmC* phase at a rate of 0.1 °C/min.

Measurement. The phase transition temperatures were determined by differential scanning calorimetry (DSC; DSC20-TS15, Mettler) and microscopic observation (FP-80, FP-82, Mettler; BX-50 polarizing microscope, Olympus).

The photorefractive effect was measured in a two-beam coupling experiment. A linearly polarized beam from an Ar^+ laser (165LGS-S, Laser Graphics; 488 nm, continuous wave) was divided in two by a beam splitter and was then interfered to the sample film. A *p*-polarized beam was used in most of the experiments in this study. The intensity of the laser was 2.5 mW for each beam (1-mm diameter). The laser incidence geometry is shown in Figure 2. The sample was thermostated (30 °C) using a thermocontroller (DB1000, Chino Co.). An electric field of 0−10 V/μm was applied to the sample from a regulated DC power supply (Kenwood DW36-1), and the change in the transmitted beam intensity was monitored by photodiodes (ET-2040, Electrooptics Technology, Inc.) and recorded by a computer. The refractive index grating formation time in the FLC was measured on the basis of the simplest single-carrier model of photorefractivity,[2,3] in which the gain transient is exponential. The rising signal of the two-beam coupling was fitted by a single-exponential function.

Results and Discussion

Two-Beam Coupling Experiment Using FLCs. Figure 3 shows a typical example of the asymmetric energy exchange observed in the SCE8/CDH/TNF sample under an applied DC

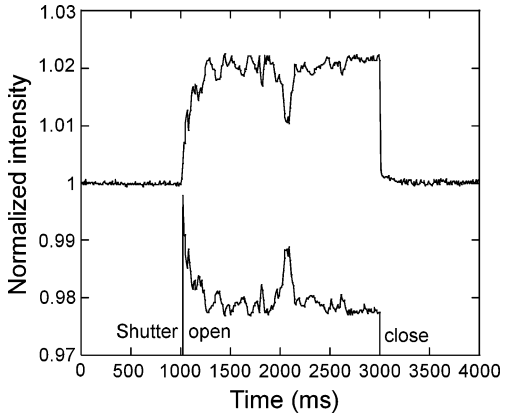

Figure 3. Typical example of asymmetric energy exchange observed in SCE8 mixed with 2 wt % CDH and 0.1 wt % TNF. The sample angle, α, was 50°, and the intersection angle, ϕ, was 20°. An electric field of +0.3 V/μm was applied to the sample.

electric field of 0.1 V/μm. Interference of the divided beams in the sample resulted in increased transmittance of one beam and decreased transmittance of the other. The change in transmitted intensities of the two beams is completely symmetric, as can be seen in Figure 3. This result indicates that the phase of the refractive index grating is shifted from that of the interference fringe.[1−3] To calculate the two-beam coupling gain coefficient, the diffraction condition needs to be correctly identified. The two possible diffraction conditions are the Bragg regime and the Raman−Nath regime, distinguished by the dimensionless parameter Q as follows.[2]

$$Q = 2\pi\lambda L/n\Lambda^2 \tag{1}$$

where L is the interaction path length. The spacing of the interference fringe (Λ) was 1.9 μm inside the material. The Bragg regime of optical diffraction is defined as $Q > 1$ and excludes multiple scattering to produce only one order of diffraction of light. Conversely, $Q < 1$ is defined as the Raman−Nath regime of optical diffraction, in which many orders of diffraction can be observed. A Q value of greater than 10 is usually required to guarantee that diffraction occurs entirely in the Bragg regime. In the present experimental condition, the Q value exceeded 10 at the intersection angles (ϕ) larger than 30°. The two-beam coupling gain coefficient Γ was calculated assuming Bragg diffraction, as follows.[1,2]

$$\Gamma = \frac{1}{L}\ln\left(\frac{gm}{1+m-g}\right) \tag{2}$$

where g is the ratio of intensities of the signal beam behind the sample with and without a pump beam, and m is the ratio of the beam intensities (pump/signal) in front of the sample. At $\phi = 20°$, the Q value was calculated as 6.2. Therefore, the diffraction observed at $\phi = 20°$ occurs predominantly, but not entirely, in the Bragg regime, with a small Raman−Nath component. However, since higher-order diffraction was not observed, Γ at $\phi = 20°$ was calculated according to eq 2.

Effect of the Thickness of the FLC Film. Figure 4 shows the dependence of the gain coefficient on the thickness of the

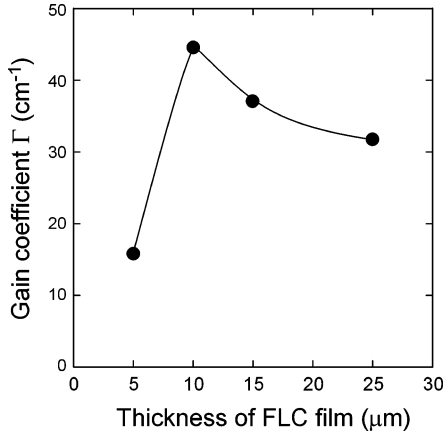

Figure 4. Dependence of the gain coefficient of the FLC/CDH/TNF mixture on the thickness of the FLC film. The sample angle, α, was 50°, and the intersection angle, ϕ, was 30°. An electric field of +0.3 V/μm was applied to the sample.

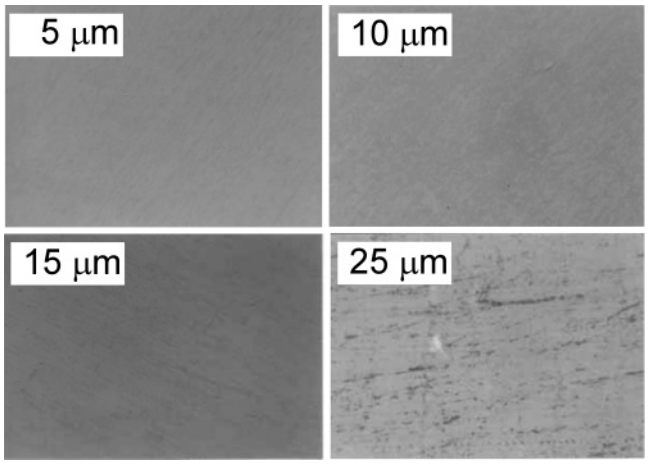

Figure 5. Textures of SS-states for FLC films observed under a polarizing microscope.

FLC film. FLC samples with film thicknesses of 5−25 μm were prepared. The gain coefficient of the 10-μm sample was 3 times larger than that of the 5-μm sample. The small gain coefficient of the 5-μm sample is caused by the shorter optical path length. The optical interaction path in the 5-μm sample, under the present beam incidence condition, is not sufficiently long for a beam coupling. The gain coefficient attained a maximum value at a film thickness of 10 μm and then decreased with increasing thickness to 25 μm. The surface-stabilized state (SS-state) of FLC is formed through interactions between FLC molecules and the surface of the polyimide alignment layer.[23,24] FLC molecules are adsorbed on the surface of the polyimide layer and the binding force propagates from the adsorbed FLC molecules to the FLC molecules in the bulk. Thus, the thickness of the FLC film has a strong affect on the quality of the SS-state. The thickness of SS-FLC films in display applications is typically 2 μm, and in such thin films the FLC molecules can form a simple book shelf structure.[23] However, in thicker films, the SS-state is not a simple one and several structures coexist.[25]

The photographs of the textures of those FLC samples observed under polarizing microscope are shown in Figure 5. The FLC used in this study provides a highly homogeneous SS-state at a film thickness (cell gap) up to 10 μm; however, the homogeneous quality of the SS-state is lowered in films thicker than 15 μm, and defects appear in the texture of these thick films. In previous work performed, the homogeneity of the SS-state strongly affected the photorefractivity.[18] The

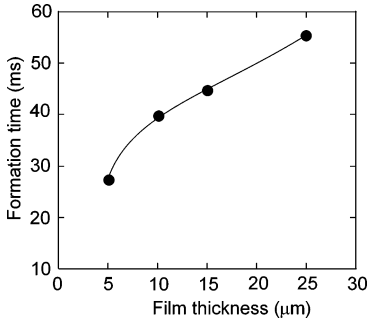

Figure 6. Dependence of the refractive index grating formation time, in the FLC/CDH/TNF mixture, on the thickness of the FLC film. The sample angle, α, was 50°, and the intersection angle, ϕ, was 30°. An electric field of +0.3 V/μm was applied to the sample.

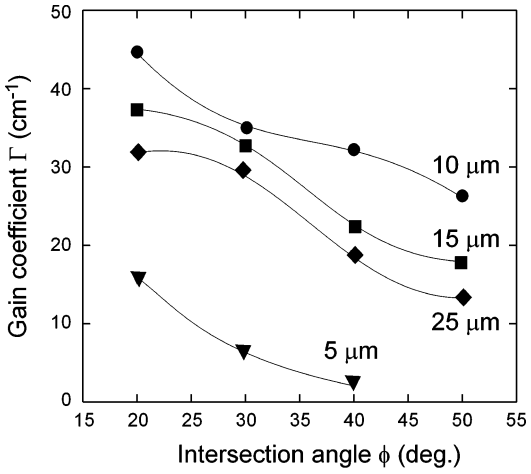

Figure 7. The gain coefficient of the FLC/CDH/TNF mixture as a function of the intersection angle, ϕ. The sample angle, α, was set to 50°. An electric field of +0.3 V/μm was applied to the sample.

presence of defects in the SS-state results in a noisy signal for the two-beam coupling experiment and also reduces the gain coefficient. Therefore, the lowering of the homogeneity of the SS-state in thicker samples leads to a lower gain coefficient. There are many reports regarding the relationship between the properties of the SS-state and the film thickness.[23] FLCs form a helical phase structure in the Sc* phase for a sufficiently thick film; however, when the film is thinner than the critical thickness, the FLC molecules form an SS-state. The critical film thickness is determined by the elastic energy and the surface energy, so that for FLCs with a larger critical thickness, thicker films with a homogeneous SS-state can be prepared and will be able to provide a larger gain coefficient.

The dependence of the refractive index grating formation time on the thickness of the FLC film is shown in Figure 6. The formation time increases with the film thickness. As described above, the binding force from the glass surface on the FLC molecules in the bulk is to some degree smaller in a thicker film. Spontaneous polarization of a unit volume in the film is reduced for a thicker film and gives a slower response to an internal electric field.

Effect of the Intersection Angle of the Beams. The effect of the beam incidence condition on the magnitude of the gain coefficient was investigated. The gain coefficients for several thicknesses of FLC samples were measured as a function of the intersection angle (ϕ) of the beams, and the results are presented in Figure 7. A decrease in the gain coefficient was observed with increasing intersection angle. With increasing intersection angle, the spacing of the interference fringe narrows. The intersection angle dependence was almost the same for all

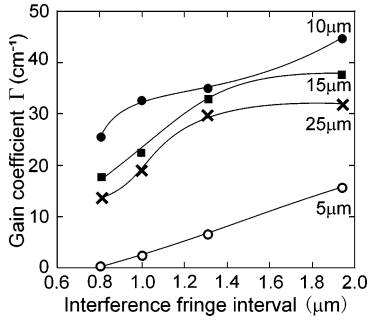

Figure 8. The gain coefficient as a function of the spacing of the interference fringe. The sample angle, α, was 50°. An electric field of +0.3 V/μm was applied to the sample.

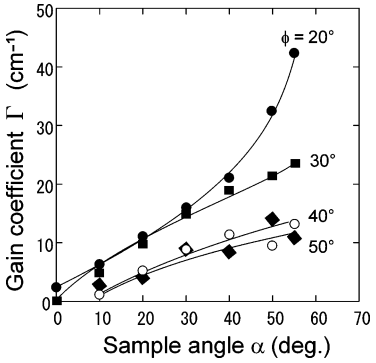

Figure 9. The gain coefficient of the FLC/CDH/TNF mixture as a function of the sample angle, α. The intersection angle, ϕ, was set to 20°. An electric field of +0.3 V/μm was applied to the sample.

film thicknesses. The magnitude of the gain coefficient, as a function of the spacing of the interference fringe (Λ), is shown in Figure 8. Thus, the dependence on the intersection angle can be attributed to the resolution of the refractive index grating. The maximum resolution of 0.8 μm was obtained in this sample.

Several studies on the photorefractivities of nematic phase LCs have been reported, where the resolution of refractive index grating is low because of the multidomain structure.[9−14] Some of these studies indicate that only polymer stabilized nematic LCs can form a Bragg diffraction grating.[11−13] In many cases, nematics are used in homeotropic alignment for photorefractivity studies. Although the homeotropic state is apparently transparent, the phase is composed of numerous small domains and because of the fluid nature of nematic LCs, the directors of those domains fluctuate and cause dynamic light scattering. The formation of an internal electric field and orientational grating is affected by the multidomain structure and results in the low resolution of the grating. Compared to nematic LCs, smectic phase LCs are more crystalline than liquid, so that the smectic LC films are highly transparent. A refractive index grating in the Bragg regime is readily formed in SS-FLCs.

Effect of the Sample Angle. The dependence of the gain coefficient on the sample angle (α) is shown in Figure 9. The gain coefficient increased with the sample angle, up to a maximum at 55°, which is the largest angle available with the experimental apparatus. The change in the sample angle yields a change in the optical path length within the FLC film, in addition to the angle between the interference fringe wave vector and the external electric field. The length of the optical path within the FLC film increases with the sample angle. Therefore, the increase in the gain coefficient may originate from the increase in the interaction path length of the beams and the increased intensity of the external electric field component along the interference wave vector (the direction of charge separation).

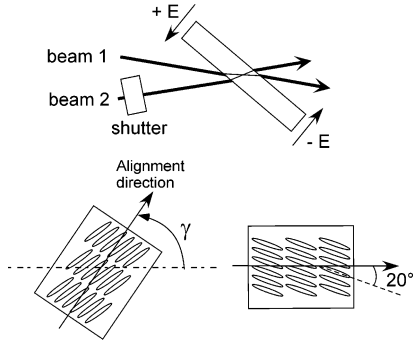

Figure 10. The sample rotation angle, γ, and the definition of the direction for the external electric field (+E and −E).

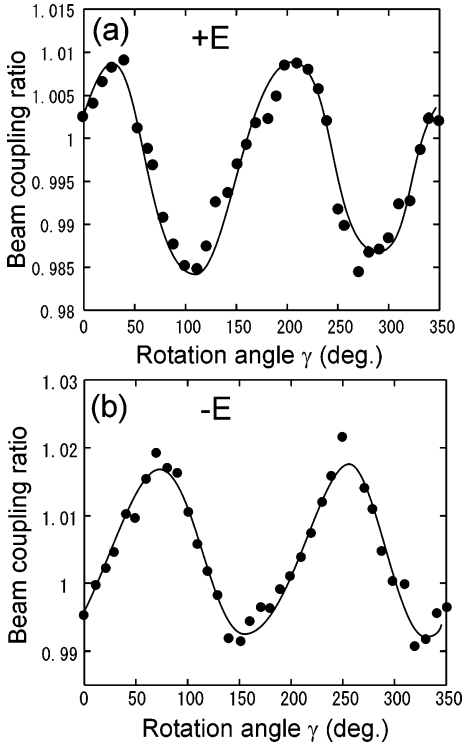

Figure 11. Dependence of the beam coupling ratio, in a two-beam coupling experiment using *s*-polarized beams, on the sample rotation angle. (a) An electric field of +0.3 V/μm was applied to the sample. (b) An electric field of −0.3 V/μm was applied to the sample. The film thickness was 10 μm. The sample angle, α, was 50°, and the intersection angle, ϕ, was 20°.

Effect of the Beam Polarization and the Rotation Angle of the Sample. SS-FLC films possess a large optical anisotropy; therefore, the influence of the angle between the polarization direction of the laser beam and the alignment direction of FLC molecules is significant. The dependence of the beam coupling ratio in the two-beam coupling experiment is plotted as a function of the sample rotation angle (illustrated in Figure 10) in Figures 11 and 12, for *s*-polarized and *p*-polarized beams, respectively. The beam coupling ratio (r_0) is defined as a ratio of the transmitted intensity of beam 1 with transmission of beam 2 (pump beam) to the transmitted intensity without pump beam ($r_0 = I_{\text{withpump}}/I_{\text{withoutpump}}$). When the value of the coupling ratio is higher than 1.0, the intensity of beam 1 is amplified and that of beam 2 is reduced. On the other hand, when the value of the coupling ratio is lower than 1.0, the intensity of beam 2 is amplified and that of beam 1 is reduced.

In the *s*-polarized beams, shown in Figure 11, the beam coupling ratio showed a sinusoidal dependence on the sample rotation angle. The coupling ratio gave peak values at ap-

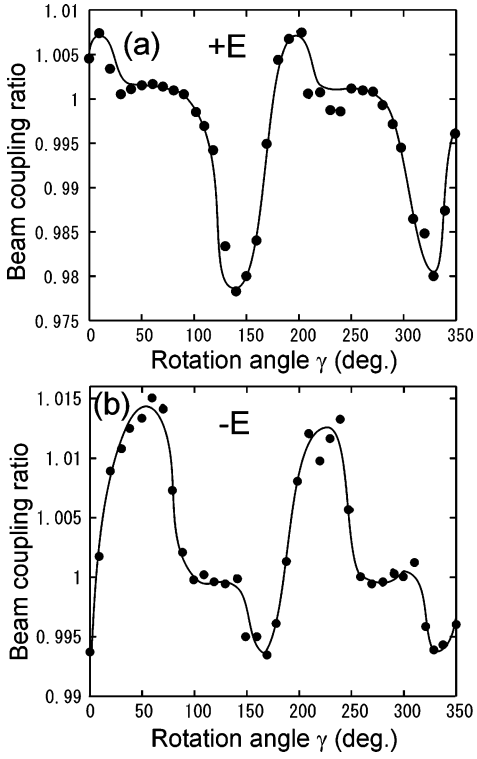

Figure 12. Dependence of the beam coupling ratio, in a two-beam coupling experiment using *p*-polarized beams, on the sample rotation angle. (a) An electric field of +0.3 V/μm was applied to the sample. (b) An electric field of −0.3 V/μm was applied to the sample. The film thickness was 10 μm. The sample angle, α, was 50°, and the intersection angle, ϕ, was 20°.

proximately 20°, 110°, 200°, and 290° under an electric field of +0.1 V/μm. With a reverse in the direction of the applied DC electric field, the sinusoidal curve was inverted and shifted by 40°, which is twice the tilt angle of the FLC molecule. On the other hand, when *p*-polarized beams were used, the rotation angle dependence is rather complicated, as can be seen from Figure 12. The curve in Figure 12a shows minima and maxima at approximately 20°, 140°, 200°, and 320°. The maxima for the coupling ratio at 20° and 200° are the same as for those of the *s*-polarized beams (Figure 11a. However, at the sample rotation angles of 140° and 320°, the coupling ratio gave minimum values (+E, Figure 12 a), and at 50° and 230° (−E, Figure 12b), the direction of either the long axis or the short axis of FLC molecules did not coincide with the polarization planes of the beams.

The rotation of beam polarization through the FLC film was investigated and the results are presented in Figure 13. Polarizers, with directions that are perpendicular to the incident beam polarizations, were placed behind the sample and the transmitted beam intensities were then measured. The laser was *p*-polarized and an electric field of − 0.3 V/μm was applied; the same conditions were used for the results of Figure 12b. Both of the beams were rotated to a large extent at the sample rotation angles of 50° and 230°, coinciding with the maximum peaks in the beam coupling ratio in Figure 13b. The behavior can be analyzed using optics theory for the anisotropic media; however, the treatment is complicated and will be presented elsewhere.

Effect of the Beam Intensity. The effect of the laser power on the photorefractivity was investigated. The dependence of the gain coefficients on the beam intensity is shown in Figure 14. The gain coefficient increased with the beam intensity up to 255 mW/cm^2, and then became almost constant at higher intensities. This can be explained by the refractive index grating,

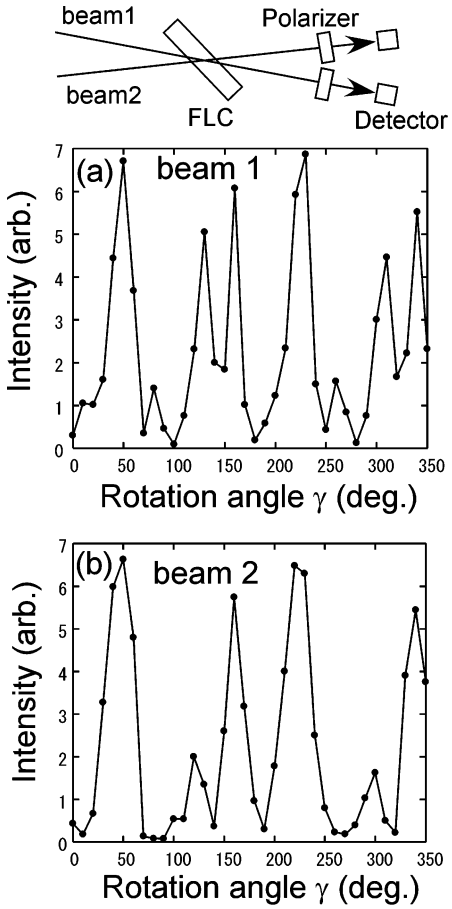

Figure 13. Transmitted intensity of the laser beams through the FLC film and a polarizer, as a function of the sample rotation angle. A *p*-polarized beam was used and an electric field of −0.3 V/μm was applied. (a) Transmitted intensity of beam 1. (b) Transmitted intensity of beam 2. The sample angle, α, was 50°, and the intersection angle, ϕ, was 20°.

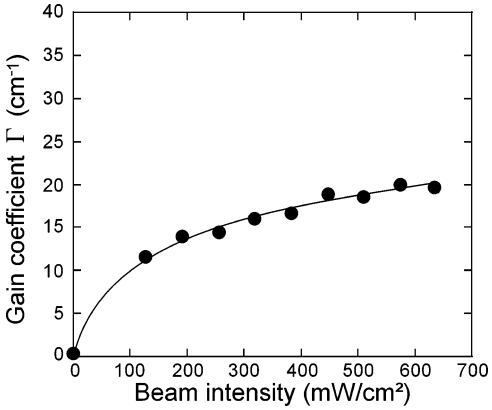

Figure 14. Dependence of the gain coefficient, of the FLC/CDH/TNF mixture, on the beam intensity. The film thickness was 10 μm. The sample angle, α, was 50°, and the intersection angle, ϕ, was 20°. An electric field of +0.3 V/μm was applied to the sample.

which is caused by the generation of a space-charge field. When the intensity of the beam is low, the strength of the space-charge field increases as the intensity increases, because of the increased amount of generated charge. The strength of the space-charge field then becomes saturated at sufficient beam intensities.

The effect of the beam intensity on the refractive index grating formation time was investigated. The formation time is plotted as a function of the intensity of the beam in Figure 15. The formation time was shortened as the intensity of the beam

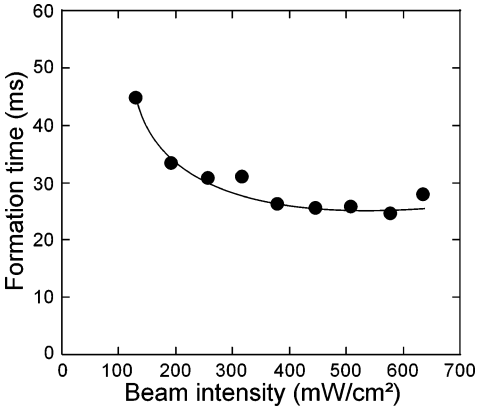

Figure 15. The index grating formation time, of the FLC/CDH/TNF mixture, as a function of the beam intensity. The film thickness was 10 μm. The sample angle, α, was 50°, and the intersection angle, ϕ, was 20°. An electric field of +0.3 V/μm was applied to the sample.

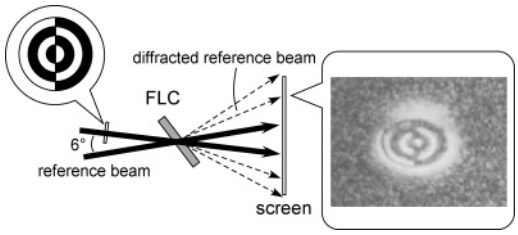

Figure 16. Photograph of an optical image diffracted by a photorefractive hologram formed in the FLC medium. An electric field of +0.3 V/μm was applied. The sample angle, α, was 50°, and the intersection angle, ϕ, was 6°.

increased, because of an accelerated formation of the space charge field, and then became constant at intensities higher than 380 mW/cm^2.

Hologram Experiment. The capturing of a photorefractive optical image in the SS-FLC was performed. The optical image and the reference beam were interfered in the sample with the Raman−Nath (thin hologram) condition, where higher order diffractions are allowed. A laser beam, transmitted through a transparent sheet printed with a pattern (object beam), was interfered with a reference beam in the FLC. A part of the reference beam was diffracted by the photorefractive hologram into the angle of higher order diffractions, and Figure 16 shows the photograph of the first-order diffraction on a screen. Clearly, the diffracted reference beam contains the image information, indicating that a hologram image was formed in the FLC medium. The photorefractive grating vanishes when the internal electric field disappears and the separated charges recombine quickly when the interference fringe disappears. Therefore, the photorefractive gratings of FLCs are considered as being reversible and can be utilized for dynamic real-time holograms.

Conclusion

The influences of several experimental conditions on the photorefractive effect of a ferroelectric liquid crystal were investigated. The effects of intersection angle of the beams, sample angle, polarization, intensities of the beams, and the thickness of the FLC sample were explored. SS-FLC samples possess a large optical anisotropy, and therefore the laser incidence condition strongly affects the photorefractivity. The response time was in the order of few tens of ms and is dominated by the formation of the internal electric field. Faster responses will be obtained by utilizing FLC materials with higher photoconductivity.

Acknowledgment. This work was supported by a Grant-in-Aid for Scientific Research from the Ministry of Education, Culture, Sports, Science, and Technology, and Research Foundation for Opto-Science and Technology.

References and Notes

(1) Solymar, L.; Webb, J. D.; Grunnet-Jepsen, A. *The Physics and Applications of Photorefractive Materials*; Oxford: New York, 1996.

(2) Yeh, P. *Introduction to Photorefractive Nonlinear Optics*; John Wiley: New York, 1993.

(3) Moerner, W. E.; Silence, S. M. *Chem. Rev.* **1994**, *94*, 127.

(4) Kippelen, B.; Peyghambarian, N. *Advances in Polymer Science, Polymers for Photonics Applications II*; Springer: 2002; pp 87−156.

(5) Meerholz, K.; Volodin, B. L.; Kippelen, B.; Peyghambarian, N. *Nature* **1994**, *371*, 497.

(6) Kippelen, B.; Marder, S. R.; Hendrickx, E.; Maldonado, J. L.; Guillemet, G.; Volodin, B. L.; Steele, D. D.; Enami, Y.; Sandalphon; Yao, Y. J.; Wang, J. F.; Röckel, H.; Erskine, L.; Peyghambarian, N. *Science* **1998**, *279*, 54.

(7) Hattemer, E.; Zentel, R.; Mecher, E.; Meerholz, K. *Macromolecules* **2000**, *33*, 1972.

(8) Wright, D.; Gubler, U.; Moerner, W. E.; CeClue, M. S.; Siegel, J. S. *J. Phys. Chem. B* **2003**, *107*, 4732.

(9) Khoo, I. C.; Li, H.; Liang, Y. *Opt. Lett.* **1994**, *19*, 1723.

(10) Wiederrecht, G. P.; Yoon, B. A.; Wasielewski, M. R. *Science* **1995**, *270*, 1794.

(11) Wiederrecht, G. P.; Yoon, B. A.; Svec, W. A.; Wasielewski, M. R. *J. Am. Chem. Soc.* **1997**, *119*, 3358.

(12) Wiederrecht, G. P.; Waiselewski, M. R. *J. Am. Chem. Soc.* **1998**, *120*, 3231.

(13) Ono, H.; Kawamura, T.; Frias, N. M.; Kitamura, K.; Kawatsuki, N.; Norisada, H. *Adv. Mater.* **2000**, *12*, 143.

(14) Wiederrecht, G. P.; Yoon, B. A.; Wasielewski, M. R. *Adv. Mater.* **2000**, *12*, 1533.

(15) Sasaki, T.; Kino, Y.; Shibata, M.; Mizusaki, N.; Katsuragi, A.; Ishikawa, Y.; Yoshimi, T. *Appl. Phys. Lett.* **2001**, *78*, 4112.

(16) Sasaki, T.; Katsuragi, A.; Ohno, K. *J. Phys. Chem. B* **2002**, *106*, 2520.

(17) Sasaki, T.; Ohno, K.; Nakazawa, Y. *Macromolecules* **2002**, *35*, 4317.

(18) Sasaki, T.; Katsuragi, A.; Mochizuki, O.; Nakazawa, Y. *J. Phys. Chem. B* **2003**, *107*, 7659.

(19) Sasaki, T.; Goto, M.; Ishikawa, Y.; Yoshimi, T. *J. Phys. Chem. B* **1999**, *103*, 1925.

(20) Sasaki, T.; Shimada, T.; Tachibana, K. *Chem. Lett.* **2002**, 324.

(21) Hofmann, U.; Grasruck, M.; Leopold, A.; Schreiber, A.; Schloter, S.; Hohle, C.; Strohriegl, P.; Haarer, D.; Zilker, S. J. *J. Phys. Chem. B* **2000**, *104*, 3887.

(22) Ostroverkhova, O.; Moerner, W. E. *Appl. Phys. Lett.* **2003**, *82*, 3602.

(23) Skarp, K.; Handschy, M. A. *Mol. Cryst. Liq. Cryst.* **1988**, *165*, 439.

(24) Fukuda, A.; Takezoe, H. *Structure and Properties of Ferroelectric Liquid Crystals*; Corona: Tokyo, 1990.

(25) Ouchi, Y.; Takezoe, H.; Fukuda, A. *Jpn. J. Appl. Phys.* **1987**, *26*, 4.